Metascience in Aerospace

https://www.aimspress.com/journal/mina

Metascience in Aerospace, 3(1): 56–76.
DOI:10.3934/mina.2026005
Received: 09 December 2025
Revised: 03 March 2026
Accepted: 12 March 2026
Published: 26 March 2026

Research Article

Magnetic-torquers-only attitude control with estimation and compensation of the residual magnetic moment

Fabricio Della Vedova[1], **María Eugenia Etcheverry**[1], **Sofía Baldoni**[1], **Juan Giribet**[1,2] **and Pablo Servidia**[1,3]*

[1] Facultad de Ingeniería, Universidad de Buenos Aires, Av. Paseo Colón 850, 1063 CABA, Argentina.
[2] Laboratorio de Inteligencia Artificial y Robótica, Universidad de San Andrés - CONICET, Vito Dumas 284, B1644BID, Victoria, Buenos Aires, Argentina.
[3] CONAE - National Commission of Space Activities, Av. Paseo Colón 751, 1063 CABA, Argentina.

* **Correspondence:** Email: pservidia@conae.gob.ar, Tel: +54-11-4331-0074;

Abstract: The estimation of the residual magnetic moment in a CubeSat controlled only by magnetic torque bars is critical to achieving accurate attitude pointing. This process can be divided into two phases: an initial ground-based estimation using a testbed to characterize the magnetic moment prior to launch and a subsequent in-orbit estimation. This work proposes a low-cost, fully autonomous in-orbit estimation and compensation approach, incorporating several improvements over recently published methods. Moreover, we present results obtained using a magnetic-only feedback control scheme, which poses additional challenges to the robustness of the combined controller-estimator-compensator system. The analysis also includes scenarios with intermittent attitude information caused by typical eclipse periods in low Earth orbits. In addition, a nadir-pointing mode is evaluated under near-inertial pointing conditions to assess the behavior of the estimator. Finally, the observability of the residual magnetic moment estimator is verified using an appropriate time-varying formulation of the innovation process.

Keywords: magnetic attitude control; boresight pointing; adaptive extended kalman filter

1. Introduction

CubeSat mission design is typically driven by low-cost strategies, which, in turn, enable the adoption of higher-risk but innovative solutions. This is particularly evident in the attitude determination and control system (ADCS) design, where diverse actuation strategies have been explored: magnetic-only actuation [1], passive control approaches [2, 3], hybrid combinations such as gravity-gradient with magnetic or aerodynamic torques [4, 5], gravity-gradient with momentum bias or control moment gyros [6], fluid dynamic actuators [7], thruster-based control [8], or magnetic control supplemented by a single

reaction wheel [9]. Moreover, new magnetic actuator implementations have been proposed to reduce cost and volume, such as the OmniMagnet [10] and the embedded asymmetric [11] concepts.

In this work, we analyze the attitude determination and control of a low cost 1U CubeSat mission concept employing magnetic actuation. Due to the low inertia of such small satellites and the disturbances caused by the residual magnetic moment (RMM), it is essential to estimate and compensate for this magnetic dipole bias in order to achieve satisfactory pointing accuracy. The RMM is typically characterized in two phases: (1) a pre-launch dipole measurement in ground tests [12], and (2) an in-orbit estimation based on onboard sensor data [13].

The main purpose of this work is to propose improvements to the magnetic dipole estimator, following [14], and to show its integration with a control system using only magnetorquers. The proposed method is evaluated under different low Earth orbit (LEO) conditions, including worst-case eclipse scenarios where Sun sensor feedback becomes unavailable. In particular, an adaptive version of the process noise covariance matrix is implemented as a function of the correction terms at each filter update step, leading to a faster convergence rate. The control law is derived from a general averaging theory [15], following the magnetic control approach proposed in [16]. Sun-pointing attitude control is achieved through the use of a partial quaternion representation as defined in [17], which is also evaluated for nadir pointing.

The structure of this work is as follows. Section 2 provides a brief overview of the satellite's objectives and main characteristics. Section 3 presents the magnetic control laws, and Section 4 introduces an enhanced formulation of the magnetic dipole estimator found in the literature. This includes an assessment of its performance under eclipse conditions, the integration of magnetic control feedback, and the implementation of an adaptive process noise covariance, together with the corresponding observability analysis. Section 5 provides the simulation results, while Section 6 summarizes the main contributions and results of this work.

2. Satellite description

This work is aligned with the ASTAR 1U Cubesat project at the University of Buenos Aires [18]. The mission objective is to test typical spacecraft operational modes for certain nominal attitudes. These objectives can be fulfilled through the following modes:

- **Detumbling:** Reduction of the satellite's angular velocity.
- **Sun pointing:** Alignment of the $+Z_b$ axis with the Sun.
- **Nadir pointing:** Alignment of the $-Z_b$ axis with the nadir.

The low-cost strategy led to the following hardware selection:

- **Structure:** 1U CubeSat format.
- **Sensors:** Coarse Sun sensor, three-axis magnetometer, three-axis gyroscope, and horizon sensor.
- **Actuators:** Three-axis magnetorquers.

Although this hardware configuration enables three control modes, the satellite's health should not depend on its attitude. Therefore, the power system incorporates solar cells on every face, and the telemetry/telecommand antenna is required to be omnidirectional. Moreover, the chosen sensors allow the spacecraft to achieve these pointing modes autonomously, without requiring feedback from the

ground segment, whose main objective is to collect telemetry information for verification purposes. Notice that, in particular, this makes the attitude determination and control independent of orbit information; the only assumption is that the orbit does not lie in the magnetic equator plane. Two possible orbital scenarios are considered: (1) an orbit with minimum inclination that allows visibility over the city of Buenos Aires (e.g., 35° inclination), and (2) a Sun-synchronous orbit, representing the maximum inclination case, with local times between 9:00hs and 15:00hs, compatible with typical rideshare launch services, for altitudes between 500km and 600km.

3. Definition of control law

3.1. Attitude kinematics and dynamics

The CubeSat can be considered as a rigid body, with an angular velocity vector $\underline{\omega} \in \mathbb{R}^3$, and an attitude representation given by the quaternion vector $Q = [q_0, \underline{q}^T]^T$, composed by the scalar part $q_0 \in \mathbb{R}$ and the vector part $\underline{q} \in \mathbb{R}^3$. The associated dynamic model is given by a system of first order ordinary differential equations:

$$\begin{cases} \dot{q}_0 &= -\frac{1}{2}\underline{q}^T\underline{\omega} \\ \dot{\underline{q}} &= \frac{1}{2}(q_0 I_3 + \underline{q}\times)\underline{\omega} \\ J\dot{\underline{\omega}} &= -\underline{\omega}\times J\underline{\omega} + T_{mag} \end{cases} \tag{3.1}$$

where $I_3 \in \mathbb{R}^{3\times3}$ is the identity matrix and $T_{mag} \in \mathbb{R}^3$ is the torque generated on the body by the reaction with the Earth magnetic field.

Following [17, 9] we define the *partial quaternion*:

$$Q^r = [q_{0r}\ \underline{q}_r^T]^T \tag{3.2}$$
$$q_{0r} = \cos(\phi_r/2) \tag{3.3}$$
$$\underline{q}_r = \sin(\phi_r/2)\underline{\eta}_r \tag{3.4}$$

associated to the pointing of a certain vector measured in body frame $\underline{o}_m$ towards a desired direction in body frame $\underline{o}_d$. The angle ϕ_r and axis $\underline{\eta}_r$ are given as:

$$\phi_r = \operatorname{acos}(\underline{o}_m^T\underline{o}_d) \tag{3.5}$$
$$\underline{\eta}_r = \frac{\underline{o}_m \times \underline{o}_d}{\|\underline{o}_m \times \underline{o}_d\|} \quad \text{for} \quad \phi_r \notin \{0, \pi\} \tag{3.6}$$

while $\underline{\eta}_r = \underline{0}_{3\times1}$ for $\phi_r = 0$, and $\underline{\eta}_r = \underline{\eta}_r^\perp$ for $\phi_r = \pi$. Here, we may take $\underline{\eta}_r^\perp$ as any unit vector perpendicular to $\underline{o}_d$.

Let $Q^s = [q_{0s}, \underline{q}_s^T]^T$ be the partial quaternion for Sun pointing. Without loss of generality, lets consider that it is required to point one canonical axis towards the Sun, so $(\underline{q}_s)_p = 0$ for a given pointing axis* $p \in \{1, 2, 3\}$. We also define the angular velocity $\underline{\omega}_s$ to satisfy $\dot{q}_{0s} = -\frac{1}{2}\underline{q}_s^T\underline{\omega}_s$ with $(\dot{\underline{q}}_s)_p = 0$, and $(\underline{\omega}_s)_i = (\underline{\omega})_i$ for $i \neq p$.

*For any vector $\underline{x}$, the *ith* component is $(\underline{x})_i$.

3.2. Relation between magnetic torque and moment

The intensity of Earth's magnetic field in LEO makes torque generation via magnetic coils a viable control method [16]. The associated control system underactuated, as the torque is constrained to be normal to the magnetic field vector. Let $\underline{b}_b \in \mathbb{R}^3$ be the magnetic field in body frame. Given any desired torque $\underline{u} \in \mathbb{R}^3$, the magnetic torque T_{mag} can be obtained as [16, 19, 20, 21]:

$$T_{mag} = \Gamma \underline{u} \quad \text{where} \quad \Gamma \triangleq \left[-\frac{\underline{b}_b \times \underline{b}_b \times}{\|\underline{b}_b\|^2} \right] \tag{3.7}$$

The associated command is the magnetic moment $\underline{m}$ sent to the coils, which for a desired torque $\underline{u}$ is computed as

$$\underline{m} = \left[\frac{\underline{b}_b \times}{\|\underline{b}_b\|^2} \right] \underline{u} \tag{3.8}$$

The magnetic moment is associated to the current flow and the section of the associated coil and is measured in Amperes-square meters (Am^2). In our notation, $(\underline{m})_i$ is the magnetic moment associated to the coil along the ith axis. The relation between the actual torque T_{mag} and the magnetic moment $\underline{m}$ is

$$T_{mag} = \left[-\underline{b}_b \times \right] \underline{m} \tag{3.9}$$

3.3. Feedback law for three magnetorquers

Here, we summarize the control law as given in [9]. Given $\epsilon, k_v > 0$ and the inertia matrix J, we select the detumbling mode torque vector $\underline{u} \in \mathbb{R}^3$ as:

$$\underline{u} \;=\; -\epsilon k_v J \underline{\omega} \tag{3.10}$$

Hence, the control (3.10) determines:

$$T_{mag} \;=\; -\epsilon k_v \Gamma(t) J \underline{\omega} \tag{3.11}$$

Following [16], we require the orbit be such that for any inertial pointing $\Gamma(t)$ becomes positive definite when averaged during enough time:

$$0 < \overline{\Gamma} \;\triangleq\; \lim_{T\to\infty} \frac{1}{T} \int_0^T \Gamma(t) dt \tag{3.12}$$

An additional integral condition is required and also evaluated by simulations:

$$\left\| \overline{\Gamma}_0 - \frac{1}{T} \int_t^{t+T} \Gamma_0(\tau) d\tau \right\| \leq k_{av} \sigma(T) \quad \forall t \geq 0 \tag{3.13}$$

where $\Gamma_0 = -\underline{b}_0 \times \underline{b}_0 \times \|\underline{b}_0\|^{-2}$, $\underline{b}_0$ is the magnetic vector in an inertial frame, $k_{av} > 0$, and σ is a positive, strictly decreasing, and continuous function defined for positive values, such that $\lim_{T\to+\infty} \sigma(T) = 0$. These conditions hold for near-polar orbits[†] under slow enough rotations (see Lemma 1 in [16]) or using

[†]This is the typical case for Earth observation.

a proportional-derivative (PD) control structure (see Proposition 1 in [16]). In the following, we will use the averaged model (see [15]) by replacing $\Gamma(t)$ with $\overline{\Gamma} = \overline{\Gamma}^T > 0$.

The analysis of the angular velocity feedback is made by using the following Lyapunov function:

$$V = \frac{1}{2}\underline{\omega}^T J^2 \underline{\omega} \tag{3.14}$$

and hence, we obtain for the averaged model (replacing $\Gamma(t)$ by $\overline{\Gamma}$ in T_{mag}; see [16] for a rigorous definition)

$$\dot{V} \leq -\epsilon k_v \lambda_{min}(\overline{\Gamma}) V \tag{3.15}$$

for any $0 < \epsilon, k_v, \lambda_{min}(\overline{\Gamma})$, where $\lambda_{min}(\cdot)$ is the minimum eigenvalue.

3.3.1. Stabilization of the partial quaternion

Once the angular velocity norm $\|\underline{\omega}\|$ is smaller than a threshold $c_\omega > 0$, the Sun pointing mode begins. It has two phases: during eclipse the same law (3.10) is implemented. If there is enough light detected by the CSS, we can compute the Sun vector in body frame and implement the following control law: (see [19]):

$$\underline{u} = -\epsilon^2 k_q J^{-1} \underline{q}_s - \epsilon k_v J \underline{\omega} \tag{3.16}$$

where the quaternion vector $Q^s = [q_{0s}, \underline{q}_s^T]^T$ to point the $+Z_b$ (i.e. $[0\ 0\ 1]^T$ in body frame) solar panel towards the Sun is computed using (3.5)-(3.4) in terms of the the unitary Sun vector in body frame $\underline{s}$ and its target pointing towards $+Z_b$.

The stability proof is made for the averaged rigid body model with the following Lyapunov function:

$$V = 2k_q\epsilon^2(1 - q_{s0}) + \frac{1}{2}\underline{\omega}^T J \overline{\Gamma}^{-1} J \underline{\omega} \tag{3.17}$$

where $\overline{\Gamma}$ is invertible due to (3.12), that is $\bar{\Gamma} > 0$. The derivative of V along the trajectories of the averaged system (replacing $\Gamma(t)$ by $\overline{\Gamma}$ in T_{mag}) is:

$$\begin{aligned}
\dot{V} &= -2k_q\epsilon^2 \dot{q}_{s0} + \underline{\omega}^T J \overline{\Gamma}^{-1} J \dot{\underline{\omega}} \\
&= -2k_q\epsilon^2 \left(-\frac{1}{2}\underline{q}_s^T \underline{\omega}_s\right) - \underline{\omega}^T J \overline{\Gamma}^{-1} \left(\underline{\omega} \times J\underline{\omega}\right) + \underline{\omega}^T J \overline{\Gamma}^{-1} \overline{\Gamma} \left(-k_q\epsilon^2 J^{-1} \underline{q}_s\right) - \epsilon k_v \underline{\omega}^T J \overline{\Gamma}^{-1} \overline{\Gamma} J \underline{\omega} \\
&= +k_q\epsilon^2 (\underline{\omega}_s - \underline{\omega})^T \underline{q}_s - \underline{\omega}^T J \overline{\Gamma}^{-1} \left(\underline{\omega} \times J\underline{\omega}\right) - \epsilon k_v \|J\underline{\omega}\|^2 \\
&= -\underline{\omega}^T J \overline{\Gamma}^{-1} (\underline{\omega} \times J\underline{\omega}) - \epsilon k_v \|J\underline{\omega}\|^2
\end{aligned} \tag{3.18}$$

Equation (3.18) is negative provided:

$$\|J\underline{\omega}\| \underline{\sigma}_{\overline{\Gamma}}^{-1} \|\underline{\omega}\| \|J\underline{\omega}\| \sin(\beta_J^*) < \epsilon k_v \|J\underline{\omega}\|^2 \tag{3.19}$$

$$\iff \underline{\sigma}_{\overline{\Gamma}}^{-1} \|\underline{\omega}\| \sin(\beta_J^*) < \epsilon k_v \tag{3.20}$$

$$\iff 0 < \|\underline{\omega}\| < \frac{\epsilon k_v \underline{\sigma}(\overline{\Gamma})}{\sin(\beta_J^*)} \tag{3.21}$$

where β_J^* is the maximum angle between $\underline{\omega}$ and $J\underline{\omega}$ (an explicit formula is given in [26, 19, 9]). The bound (3.21) can be found to be around five times the orbital angular velocity (see [19]). This also guarantees the asymptotic stability using the invariant set theorem (see [19]). In fact, it is not possible to maintain the condition $\dot{V} = 0$, equivalent to $\underline{\omega} = \underline{0}$, with a nonzero partial quaternion error, as it would imply a nonzero proportional feedback and therefore a nonzero angular velocity which contradicts the condition $\dot{V} = 0$. Moreover, it is easy to show that the averaged version of the system (3.1) is locally exponentially stable; hence, following the same arguments in [16], we also obtain a local exponential stability of the original system (3.1). Notice that this model does not have external disturbances as the residual magnetic moment, aerodynamic torque, and solar radiation pressure, so this will be evaluated through simulations.

3.3.2. Partial quaternion for nadir pointing

A nadir pointing may be useful for Earth observation objectives, called *boresight pointing* in [28, 29], or may be also used as zenith pointing of the opposite axis (for astronomy, cold sky calibration, etc.). Here, a boresight pointing solution is proposed by changing the control objective to point the axis $-Z_b$ toward nadir, assuming that this direction is given by an infrared horizon-sensor, even during eclipse (see [27]). As the full attitude is not available, the vector pointing is considered as *almost inertial* by using the angular velocity reference as zero in spite of the fact that the nadir is actually moving slowly one turn every orbit. This simple solution, which is validated through simulations, does not need a nonzero angular velocity reference in body frame; hence, it does not require three-axis attitude determination and control.

The condition to enter into this mode is selected near the equator during the daylight part of the orbit, in such a way that the the axis $+Z_b$ pointed to the Sun meets the initial error threshold between the opposite axis (i.e. $-Z_b$) and the nadir. This is a coarse condition which can be obtained as a function of the onboard time and the determination of the end of eclipse event as a time pattern, once it is enabled by ground command. Although this guarantees a good initial condition, during the transition, the horizon may not be available, and in this case, we use the last valid measurement of the horizon until the measurement is available again, reducing also the control gains (e.g. $\epsilon^* := \epsilon/4$).

We propose to use the same control shown for inertial pointing assuming that, for small enough torques, the same proof can be extended due to a continuity argument. Moreover, the aerodynamic and gravity gradient disturbances are reduced for this pointing. The angle around the pointed axis is left uncontrolled by construction of the partial quaternion, which avoids unnecessary control efforts. This strategy will be evaluated by numerical simulations over several orbits.

4. Residual magnetic moment estimator

Here we present an improvement of the residual magnetic moment (RMM) in-orbit estimator proposed in [14], using an extended Kalman filter with the following features:

- Nonlinear model for the prediction step.
- Magnetic feedback properly integrated in the estimator.
- Adaptive process covariance.

Finally, we evaluate the observability of the proposed solution.

The state vector to be estimated $\underline{x}$ has the angular velocity and the RMM:

$$\underline{x} = \begin{bmatrix} \underline{\omega} \\ \underline{m}^0 \end{bmatrix} \tag{4.1}$$

where $\underline{m}^0$ is the residual magnetic moment to be estimated, assumed to be constant in body frame. The continuous time non-autonomous model is defined by

$$\dot{\underline{x}} = A(\underline{x},t)\underline{x} + \underline{w} \tag{4.2}$$

where

$$A = \begin{bmatrix} J^{-1}([\underline{\omega}]_\times J - [\underline{\omega} J]_\times - \epsilon k_v \Gamma(t) J) & -J^{-1}[\underline{b}_b]_\times \\ 0_{3\times3} & 0_{3\times3} \end{bmatrix} \tag{4.3}$$

and where we have used the notation $[\cdot]_\times$ for the skew-symmetric matrix associated to the vector product.

Remark 4.1. *The matrix (4.3) does include the partial derivative relative to the derivative control term $-\epsilon k_v J^{-1}\Gamma(t)J$, which was not included in previous versions of this estimator [13, 14]. Moreover, if orbit and attitude information were available, this nonlinear prediction could include aerodynamic, sun pressure and gravity gradient torques.*

The process noise vector $\underline{w} \in \mathbb{R}^6$ is characterized by its covariance matrix $Q_k \in \mathbb{R}^{6\times6}$. The observation is the angular velocity with an additive error characterized by a covariance matrix $R_k \in \mathbb{R}^{3\times3}$. The extended Kalman filter formulation is given by:

$$\Phi_k = e^{A_k \delta_T} \tag{4.4}$$

$$G_k = \delta_T \Phi_k \tag{4.5}$$

$$\hat{\underline{x}}^-_{k+1} = \hat{\underline{x}}_k + \delta_T \begin{bmatrix} J^{-1}(-\underline{\omega}_k \times J\underline{\omega}_k + \Gamma_k \underline{u}_{k-1}) \\ 0_{3\times1} \end{bmatrix} \tag{4.6}$$

$$P^-_k = \Phi_{k-1} P_{k-1} \Phi^T_{k-1} + G_{k-1} Q_{k-1} G^T_{k-1} \tag{4.7}$$

$$H = [I_{3\times3} \;\; 0_{3\times3}] \tag{4.8}$$

$$K_k = P^-_k H^T (H P^-_k H^T + R_k)^{-1} \tag{4.9}$$

$$P_k = (I - K_k H) P^-_k \tag{4.10}$$

where $\underline{u}_k$ is the control law (3.10) or (3.16) evaluated at discrete times t_k separated by the time period δ_T; the same holds for any other vector or matrix evaluated on discrete times.

Remark 4.2. *The prediction step (4.6) actually includes the residual magnetic moment term and its compensation, so in the prediction these two terms are equal and therefore, the compensation is exact. On the other hand, the Jacobian (4.3) must include the partial derivative relative to the true residual magnetic model; hence, it is actually included on its upper-right block.*

The updated state is:

$$\hat{\underline{x}}^+_k = \hat{\underline{x}}^-_k + K_k(\underline{\omega}_k - H\hat{\underline{x}}^-_k) \tag{4.11}$$

Following [30], we propose the adaptation of the process noise covariance using the corrections:

$$Q_{k+1} = (1 - \alpha_Q)Q_k + \alpha_Q \left[(\hat{\underline{x}}_k^+ - \hat{\underline{x}}_k^-)(\hat{\underline{x}}_k^+ - \hat{\underline{x}}_k^-)^T + Q_{min} \right] \tag{4.12}$$

where $Q_{min} > 0$ guarantees a minimum singular value for this covariance, and $0 < \alpha_Q \ll 1$.

The compensation is made as follows:

$$\underline{m}^c = \underline{m} - \hat{\underline{m}}_0 \tag{4.13}$$

$$= \Gamma \underline{u} - \hat{\underline{m}}_0 \tag{4.14}$$

where $\hat{\underline{m}}_0$ has the last three components of $\hat{\underline{x}}$.

Inspired by [31], we define here a windowed observability matrix for this time-varying system with constant output matrix $H_k = H$, on the moving window $W_{k,\tau} \triangleq \{t_{k-\tau}, \ldots, t_k\}$, given $\tau \in \mathbb{N}$ as:

$$O_{k,\tau} = \begin{bmatrix} H \\ H\Phi_{k-\tau} \\ H\Phi_{k-\tau+1}\Phi_{k-\tau} \\ \cdots \\ H\Phi_k \ldots \Phi_{k-\tau+1}\Phi_{k-\tau} \end{bmatrix} \tag{4.15}$$

The observability is guaranteed, as $O_{k,\tau}$ is full rank for any k, which may be verified with the positiveness of its minimum singular value for each k, that is, the square root of the eigenvalues of the *observability grammian* $M_{k,\tau} \triangleq O_{k,\tau}^T O_{k,\tau}$. This rank condition is binary and does not directly describe the capability to estimate the RMM vector. We propose to compare the direction with worst observability, given by the eigenvector $\underline{v}_{1,k,\tau}^M$ associated to the minimum eigenvalue of $M_{k,\tau}$, with respect to the (stationary) vector to be estimated. Let us define the angle between these vectors:

$$\beta_M \triangleq \text{angle} \left\{ \underline{v}_{1,k,\tau}^M, \begin{bmatrix} \underline{0}_{3\times1} \\ \underline{m}^0 \end{bmatrix} \right\} \tag{4.16}$$

Notice that if $\beta_M \in \{0, \pi\}$, the residual momentum would not be observable. It will be shown by simulations that this angle varies around $\pi/2$ and might reach the values $\{0, \pi\}$ only on isolated times.

5. Simulation results

In this section, we show the main results using the PROPAT [32] numerical simulator in MATLAB. The simulated inertia matrix considers dominant diagonal values taken as random within 1.95 $mN \cdot m \cdot s^2 \pm 8\%$ (e.g., for a mass between 1.08kg and 1.265kg using the inertia formula for a 10cm×10cm×10cm cube):

$$J = \begin{bmatrix} 2.1 & 0.001 & -0.001 \\ 0.001 & 1.8 & -0.0001 \\ -0.001 & -0.0001 & 2 \end{bmatrix} mN \cdot m \cdot s^2 \tag{5.1}$$

where the off-diagonal elements were chosen associated to misalignment of the inertia principal axes lower than[‡] 10 mrad relative to a geometric frame aligned with the cube edges. A robustness analysis of

[‡]This bound is arbitrary, taken only to define a possible inertia matrix realization.

the proposed control law under uncertainty on the off-diagonal inertia elements is out of the scope of this work, but similar simulation results have been obtained for 100mrad of misalignment of the inertia matrix eigenvectors, which can be achieved simply by statically balancing the center of gravity.

Beyond the residual magnetic moment, other simulated disturbance models were the aerodynamic, solar radiation pressure (SRP), and gravity gradient torques:

$$T_{adn} = -\frac{1}{2}\rho\|\underline{v}_b\|^2 \cdot C_{adn} \cdot A_{adn} \cdot \left(\frac{\underline{v}_b}{\|\underline{v}_b\|} \times \underline{d}_{adn}\right) \tag{5.2}$$

$$T_{srp} = -\frac{I_{srp}}{c} \cdot C_{srp} \cdot A_{srp} \cdot \left(\frac{\underline{s}_b}{\|\underline{s}_b\|} \times \underline{d}_{srp}\right) \tag{5.3}$$

$$T_{grv} = 3 \cdot \omega_o^2 \cdot \underline{p}_b \times J\underline{p}_b \tag{5.4}$$

where $\underline{p}_b$, $\underline{v}_b$ and $\underline{s}_b$ are respectively the spacecraft position, velocity[§] and sun vectors in body frame; $C_{adn} = 2$ and $C_{srp} = 1.3$ are respectively the drag and reflectivity coefficients; $A_{adn} = 0.01m^2$ and $A_{srp} = 0.01m^2$ are the respective aerodynamic and solar radiation pressure exposed areas; $\underline{d}_{adn}$ and $\underline{d}_{srp}$ are the distances from the respective relative position of the aerodynamic and sun pressure centers with respect to the body center of mass, choosing $\underline{d}_{srp} = [7.1 \;\; 7.1 \;\; 0]^T$mm, $\underline{d}_{adn} = [5.8 \;\; -5.8 \;\; 5.8]^T$mm in the simulations; $I_{srp} = 1358W/m^2$ is the solar flux intensity; $c = 3 \cdot 10^8 m/s$ is the speed of light; and ω_o is the orbit angular velocity. We adopted a circular orbit with mean altitude of 620km and 35° inclination, while the atmospheric density model was taken from [33] and validated with Tables 4-8 in [34].

The control law implementation has the parameters given in Table 1. Notice that during the Sun pointing, a higher value for ϵ was chosen during eclipse, due to the fact that the Sun vector is not available (so that $k_q = 0$), and therefore more control authority is available for the angular velocity feedback. Finally, as the initial horizon error is bounded due to the mode transition strategy, a higher ϵ value was chosen for nadir pointing in order to attain a better stationary behavior. Empirical approaches to validate these parameters can be achieved with a motion simulator in [35], but this is out of the scope of our project and associated resources.

Table 1. Control parameters used for each attitude control mode.

Control mode	ϵ	k_v	k_q
Detumbling	0.01	0.33	0
Sun pointing and no eclipse	0.01	0.33	$2.27 \cdot 10^{-5}$
Sun pointing and eclipse	0.03	0.33	0
Nadir pointing	0.02	0.33	$2.27 \cdot 10^{-5}$

In these simulations, the magnetic moment allocation is made preserving the vector direction, as proposed in [9]. The saturation values for the magnetic actuators are 0.1Am^2 for all axes, and the residual moment is assumed lower than 0.3% of these full scale values. The eigenvalues of $\frac{1}{T}\int_0^T \Gamma(t)dt$ were evaluated, being the minimum one larger than 0.3 for all time after the first minutes of flight, which validates the averaging hipothesis (3.12).

[§]In the model of T_{adn}, we neglected the velocity of the air compared to the much higher orbital velocity in LEO.

Figure 1 shows the result for a constant RMM given by

$$\underline{m}^0 = \begin{bmatrix} -0.0003 \\ 0 \\ +0.0003 \end{bmatrix} \mathrm{Am}^2 \tag{5.5}$$

which is correctly identified after two orbits, and the lower figure shows the associated covariance. After orbit two, the control mode is sun pointing, whereas after orbit four, the controller mode is nadir pointing. Notice that these two events lead to higher estimation error for the magnetic moment.

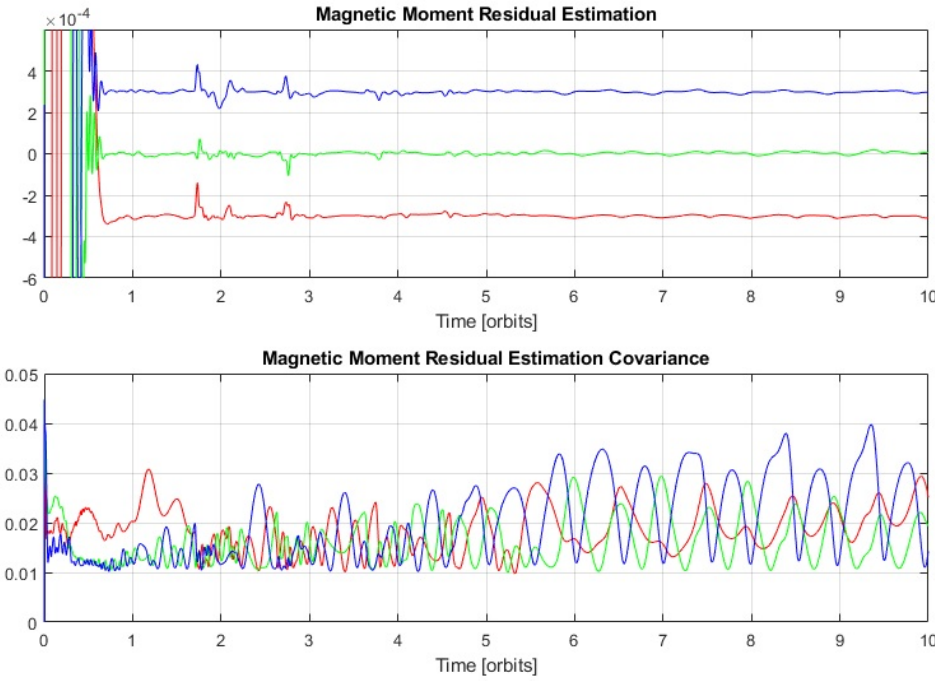

Figure 1. Residual magnetic moment estimation (upper) and related covariance (bottom).

The chosen orbit and satellite parameters resulted in similar levels of gravity-gradient, SRP, and aerodynamic disturbance torques. On the other hand, the disturbance torque due to RMM is one order of magnitude higher than these values without compensation. Once compensated, the remaining effect of the RMM is comparable to the other disturbance torques, as shown in Figure 2.

Figure 3 shows the partial quaternion error, starting with the detumbling (up to two and a half orbits), the Sun pointing (notice the drift during eclipse segments within each orbit period) and the nadir pointing (since orbit four). Figure 4 shows the norm of the angular velocity and the main attitude pointing angles during the first 10 orbits. The rotation about the nadir axis is not actively controlled and therefore does not stabilize.

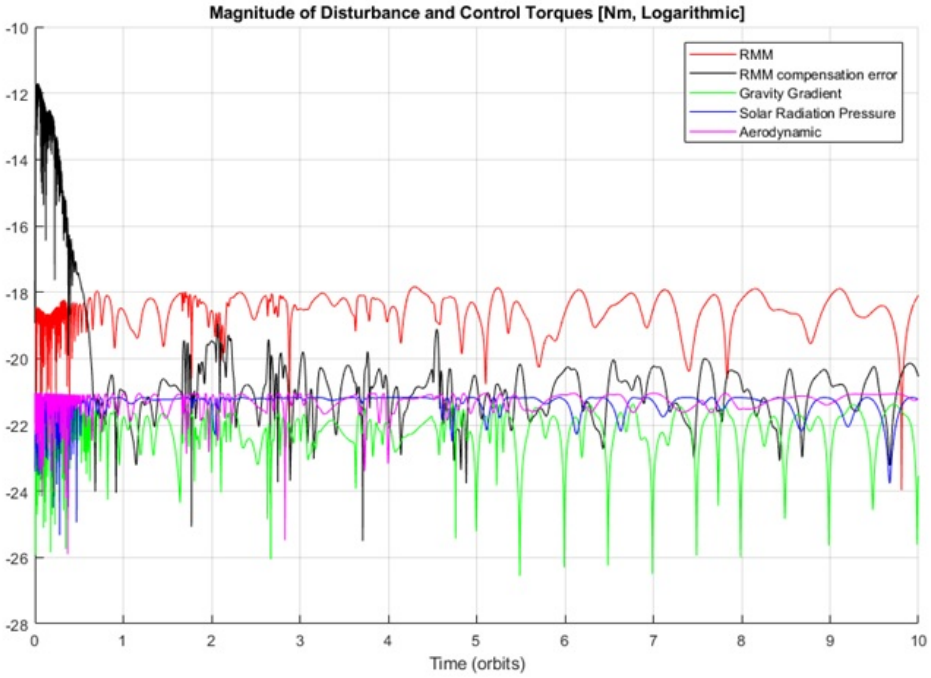

Figure 2. Logarithm of main disturbance torques.

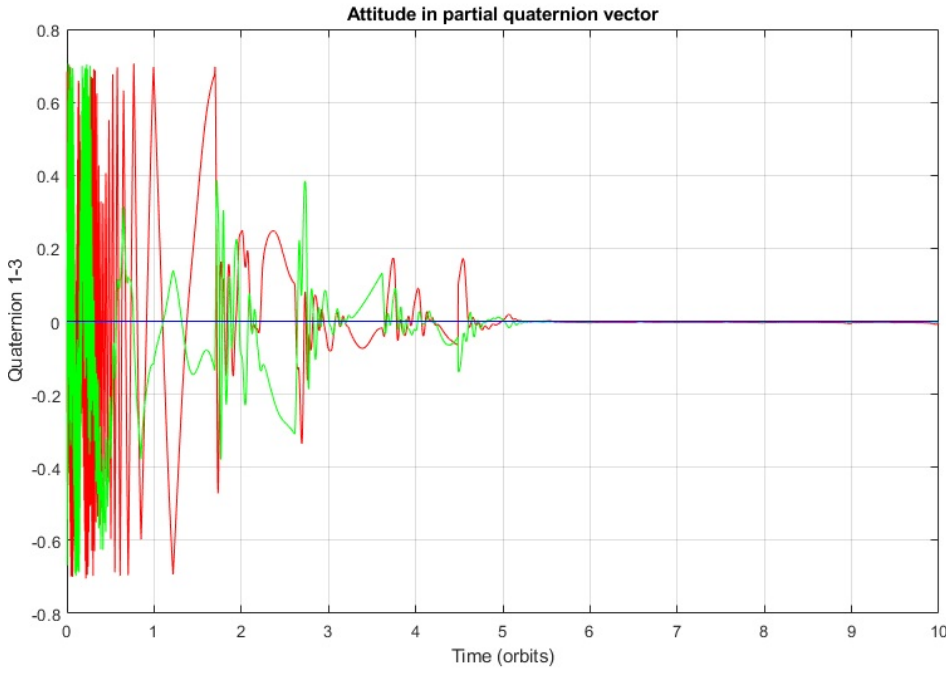

Figure 3. Components of vector part of the partial quaternion: q_1 (red), q_2 (green) and Q_3 (blue, always in zero). It is changed from Sun pointing to nadir pointing when the attitude control mode is changed similarly (after ≈ 4.5 orbits).

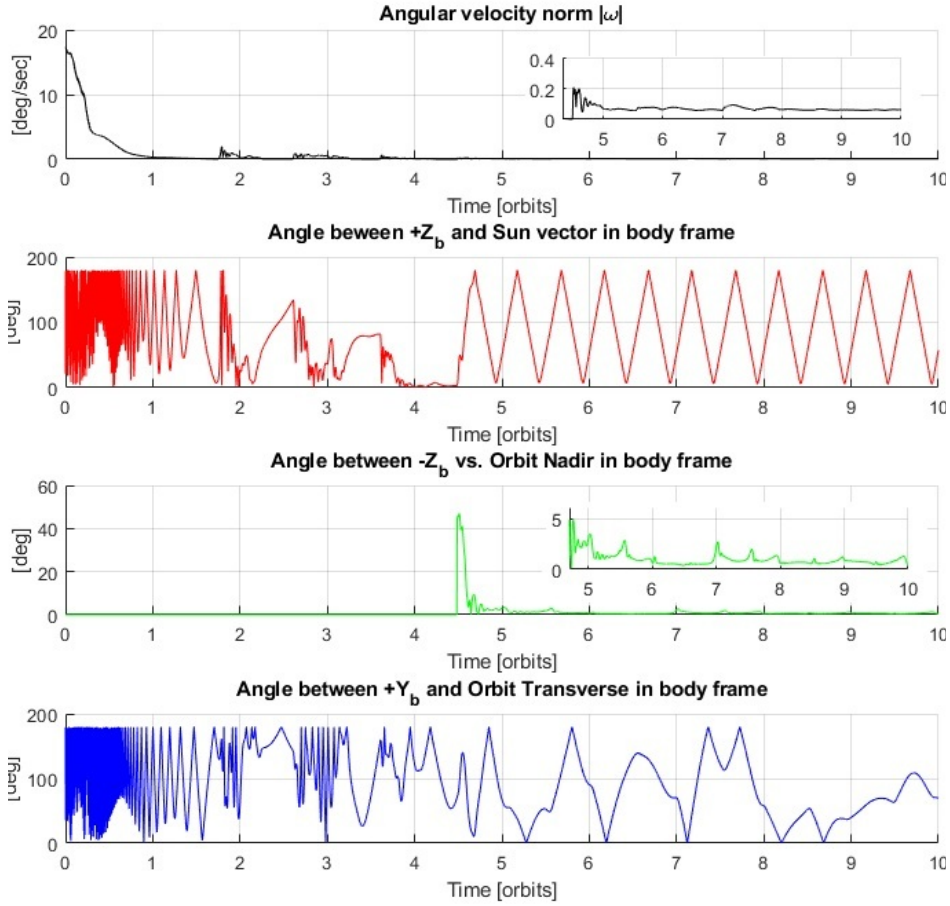

Figure 4. Angular velocity and pointing errors along the first 10 orbits, with 35° inclination at 620km. The angle between $+Y$ and the orbit transverse is not stable, whereas $-Z$ converges to nadir within approximately ±3°.

In order to check the observability condition, we evaluate the minimum singular value of $O_{k,\tau}$, shown in Figure 5. Notice that for $\tau > 2$, sufficient observability for the first orbit can be guaranteed, where the estimation task is more significant. For instance, the condition

$$\log\left(\sqrt{\underline{\lambda}(O_{k,6}^T O_{k,6})}\right) > -10 \tag{5.6}$$

was verified over ≈ 90% of the whole simulation time, where $\underline{\lambda}(M)$ is the minimum eigenvalue of a square matrix M.

The condition number of the observability grammian $O_{k,\tau}^T O_{k,\tau}$ was evaluated to confirm the numerical stability of this computation for $\tau = 6$, resulting a logarithm value between 10 and 20 during the first orbit and lower than 27 over all the ten orbits. As expected, these figures of merit improve with increasing τ. In [31], it was pointed out that rank conditions are not informative enough, so we follow a similar reasoning to evaluate the angle β_M as defined in (4.16): the result is shown in Figure 6, where it can be seen that this angle varies around $\pi/2$. This was confirmed after several attempts to identify the *worst-case* RMM direction, but the direction of the worst observability is always varying, and hence, the observability is guaranteed over the simulation time.

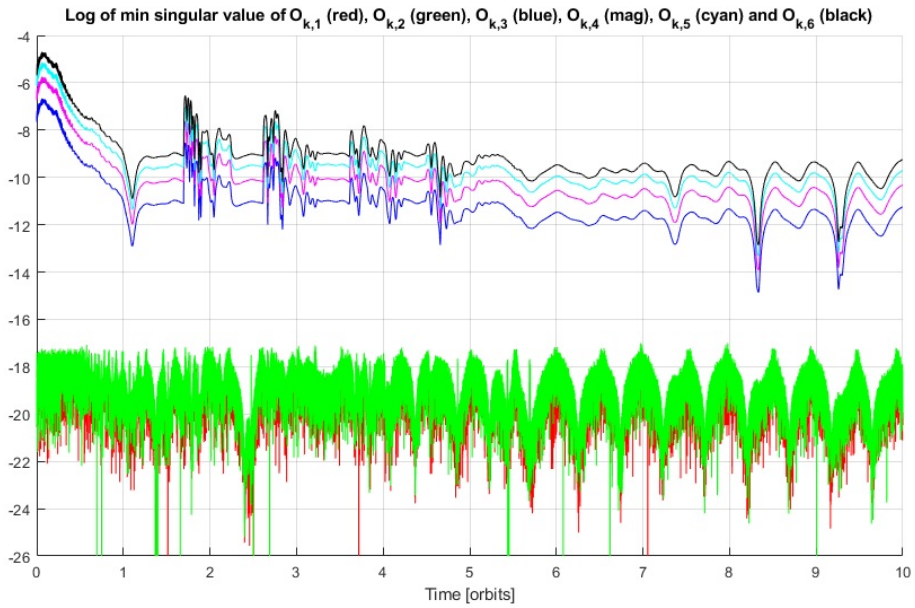

Figure 5. Minimum singular value of the windowed observability matrices $O_{k,1}, \cdots, O_{k,6}$.

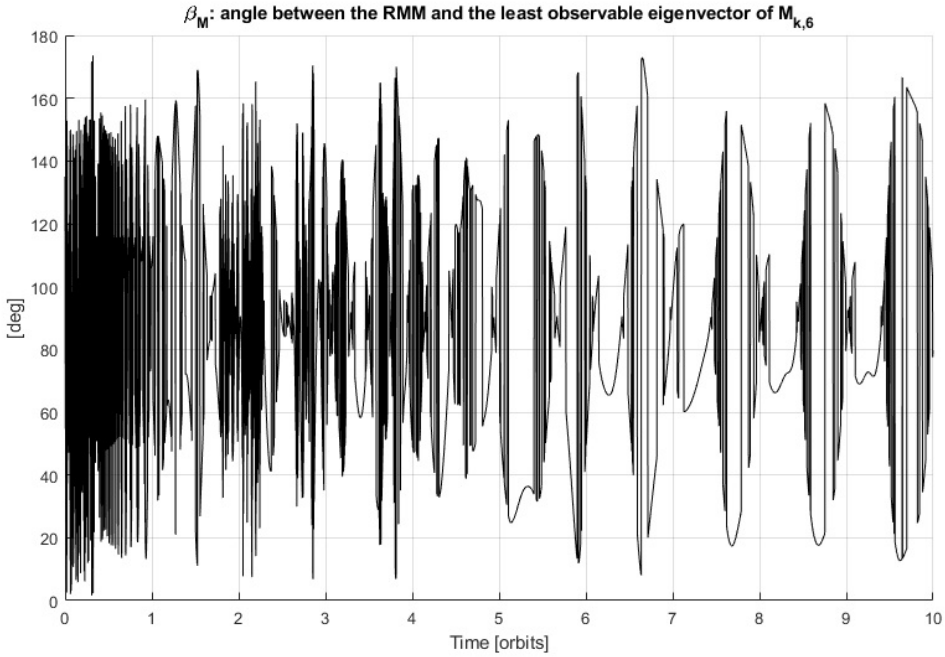

Figure 6. β_M angle for $M_{k,6}$.

The adaptive process covariance matrix (4.12) evolves as shown in Figure 7, showing an increase in Q_k when the estimation error is higher, whereas Q_k asymptotically converges to the minimum specified value (equal to the initial condition Q_0) using $\alpha_Q = 0.001$. On the other hand, it was verified by simulations that the proposed implementation achieves faster and smoother convergence of the estimation, as shown in Figure 8, without adaptation and using the same parameters as in previous simulations:

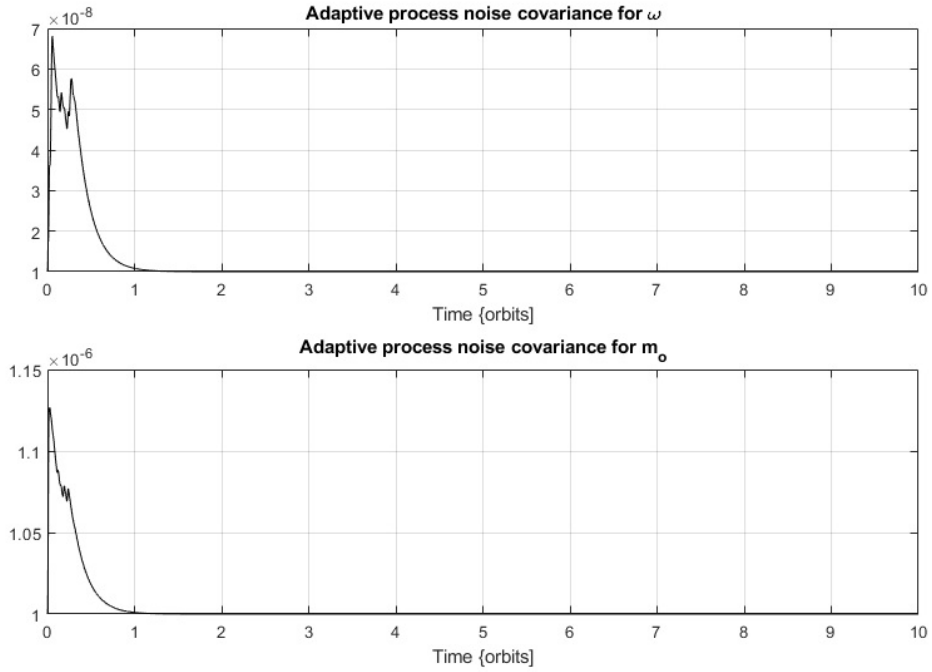

Figure 7. Minimum over x, y, z of the components of process noise covariances associated to $\underline{\omega}$ (upper) and $\underline{m}_0$ (bottom), respectively.

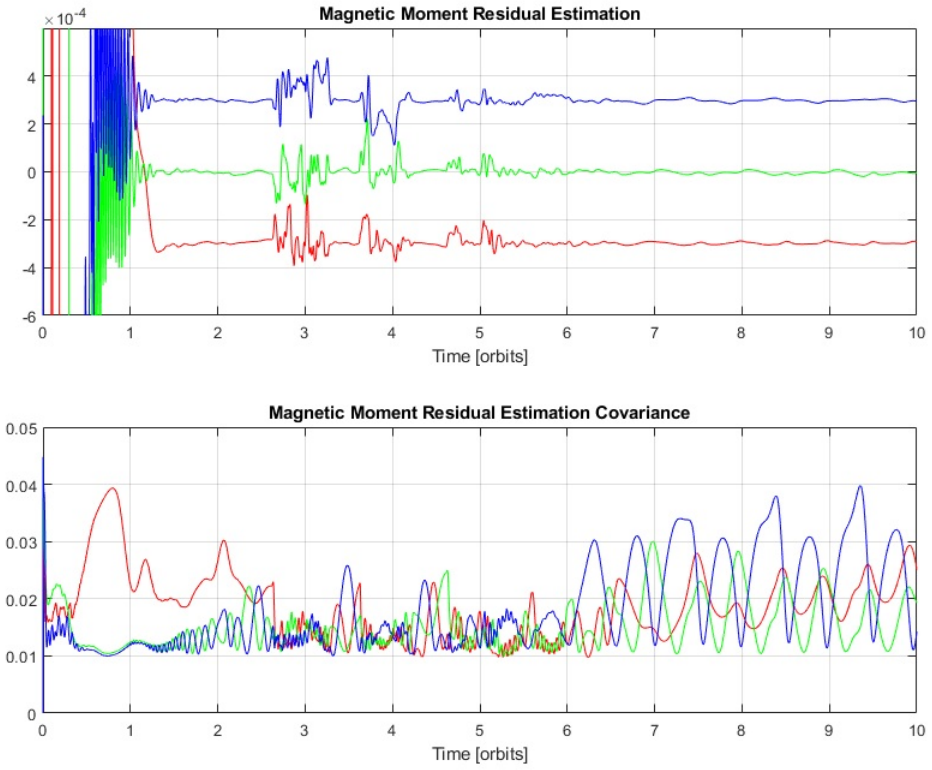

Figure 8. Residual magnetic moment estimation (upper) and related covariance (bottom), nonadaptive case.

Moreover, the resulting partial quaternion error also needs more time to converge to the sun pointing for the nonadapted process covariance estimator, as shown by Figure 9.

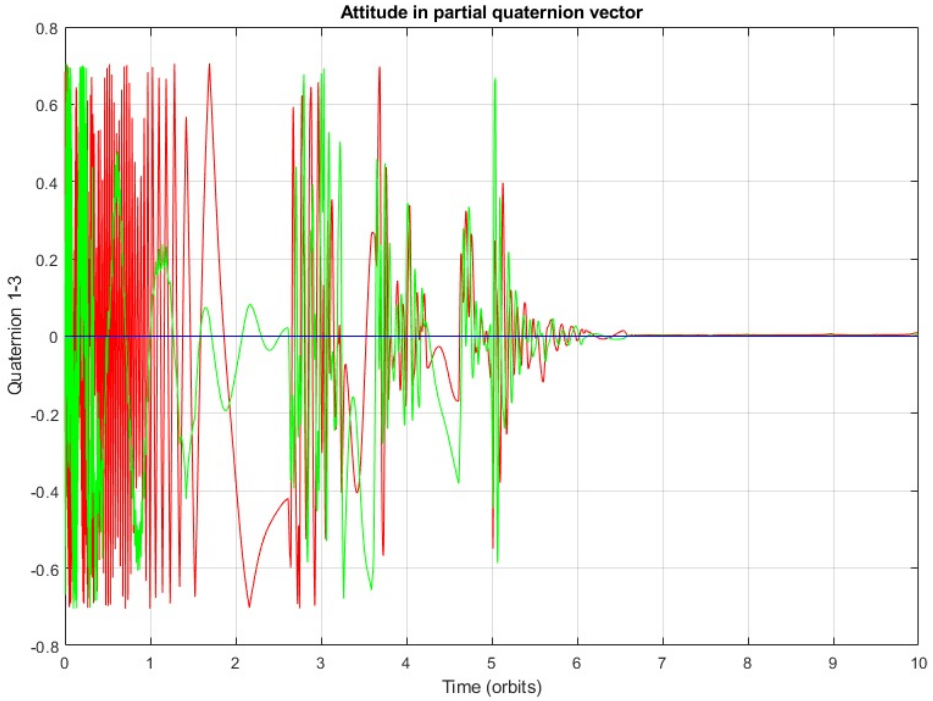

Figure 9. Components of vector part of the partial quaternion, nonadaptive case: q_1 (red), q_2 (green) and Q_3 (blue, always zero).

An assessment of the robustness of the solution was made by evaluating a sun-synchronous orbit with 520km altitude, for a local hour around 9AM, which is a possible orbit on rideshare services; the pointing results are shown in Figure 10.

For lower altitudes, the result is worse in terms of accuracy of the attitude pointing and the residual magnetic moment identification, which is due to the fact that the aerodynamic disturbance torque increases significantly. However, the concept is robust enough to keep a coarse nadir pointing. As the transition between Sun pointing and nadir pointing will occur during the first orbits after launcher separation, the horizon sensor will be tilted as a function of a lower bound on the initial orbit altitude. Using the formula for the horizon sensor boresight angle relative to nadir, as given in [27],

$$\theta_{hor} \quad = \quad \text{asin}\left(\frac{R_E}{R_E + H_o}\right) \tag{5.7}$$

where $R_E = 6378$km and H_o is the mean orbit altitude; we obtain $\theta_{hor} = 68°$ for $H_o = 500$km, and the the axis with the larger field of view should be mounted vertically (i.e., 90° on the vertical axis and 80° on the horizontal axis, following the product identification document given in [27]).

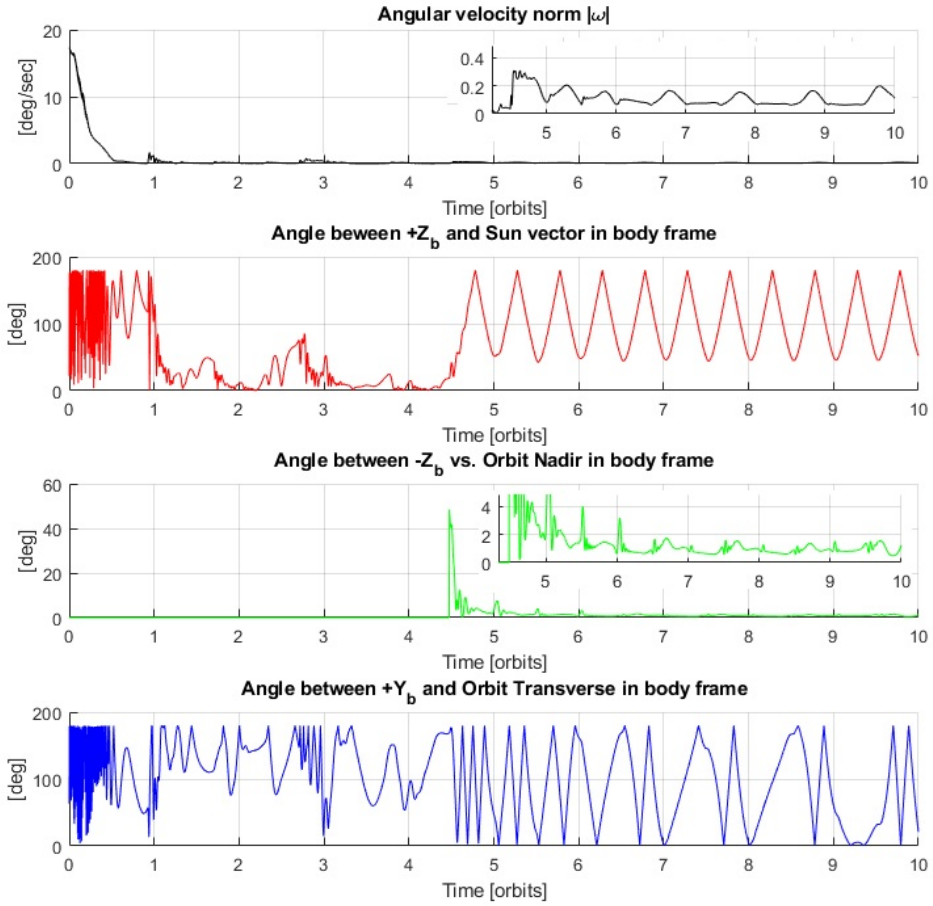

Figure 10. Pointing results for a 520km Sun synchronous orbit with local hour around 9AM.

Figure 11 shows the sensitivity of the (full) attitude quaternion error for the nadir pointing and the Sun pointing, comparing two solutions with initial conditions separated by only 1km in the semi-major axis. Notice that the third axis (blue) behavior shows a clear separation between the two solutions, whereas the first and second axes (red and green) remain very close. This sensitivity to initial conditions is indicative of chaotic dynamics, typically associated with a positive maximum Lyapunov exponent (see [36]) during (part of) the stationary regime. Notice that in the case of the nadir pointing, there is an intermittent separation behavior, whereas for the Sun pointing (which includes the non-autonomous feature due to the periodic eclipse condition), the separation is sustained for these particular simulations.

The transition into nadir pointing can be enhanced by keeping the last horizon measurement when the sensor does not provide a valid measurement due to its field of view limitations ($80° \times 90°$). This is particularly useful at lower altitudes, as it makes the transition criteria less restrictive, allowing to transition even if the measurement becomes unavailable due to higher disturbances, as shown in Figure 12. When the horizon was not available, the ϵ variable was reduced 4 times, as explained in subsection 3.3.2.

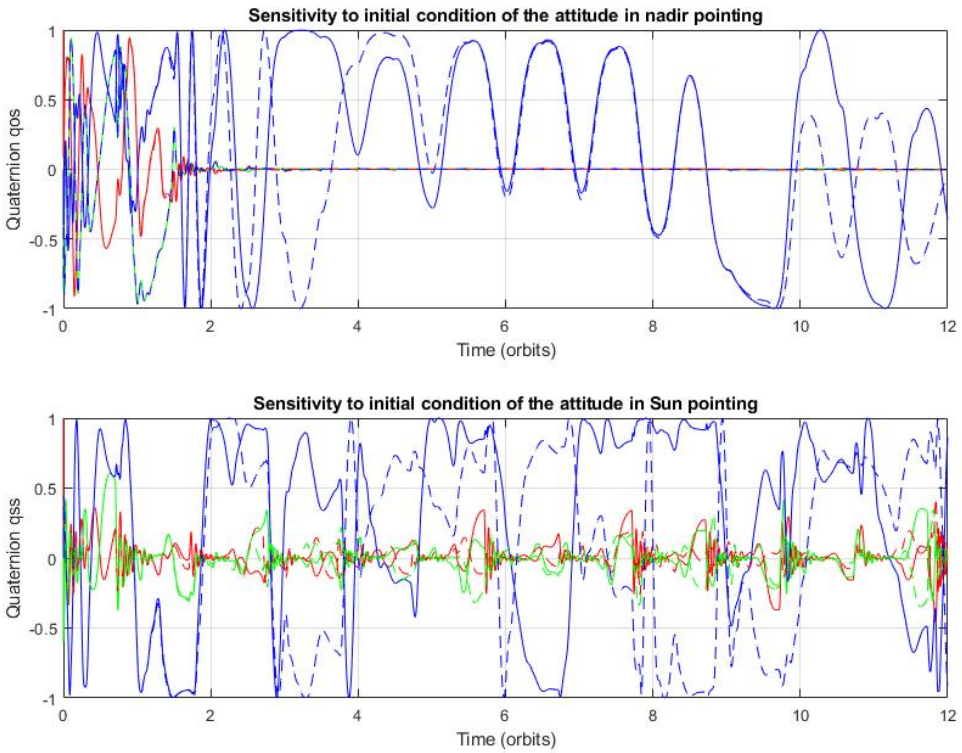

Figure 11. Sensitivity of the (full) attitude quaternion to initial conditions for the 520km Sun synchronous orbit with local hour around 9AM.

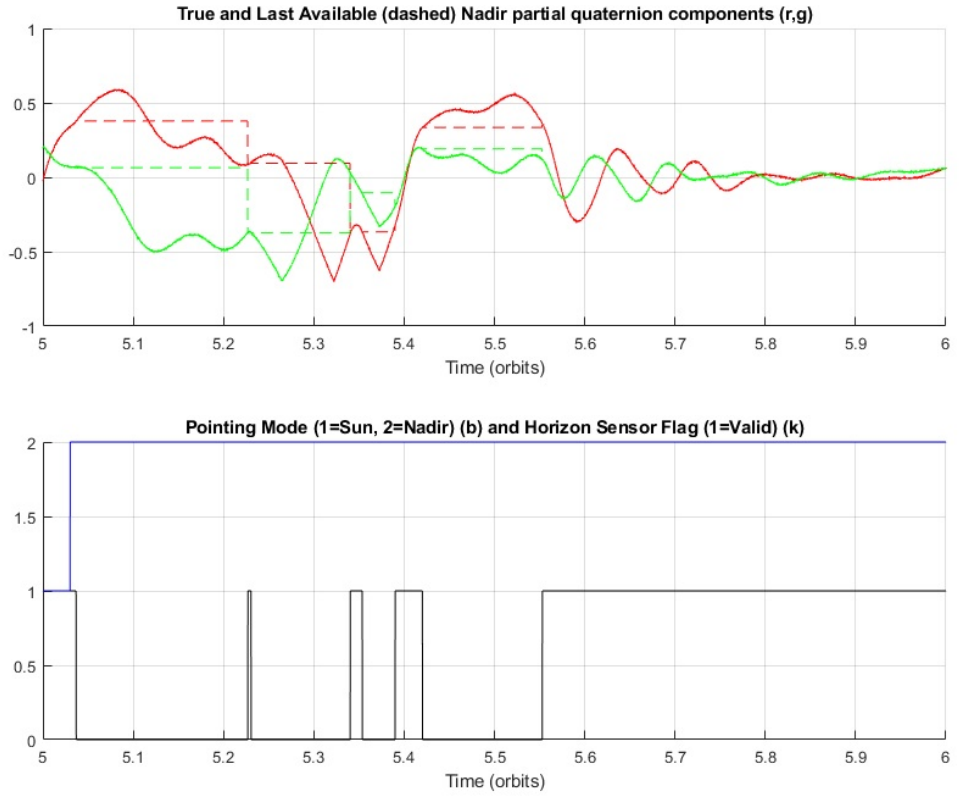

Figure 12. Transition to nadir pointing for an orbit altitude of 400km.

6. Conclusions

This work analyzes a possible configuration of sensors, actuators, and control laws for a low-cost 1U Cubesat that may achieve detumbling, Sun pointing, and nadir attitude pointing modes. Although we do not include a comparison with other solutions, it should be noted that adding reaction wheels and three-axis attitude determination (with a star tracker, GNSS receiver, and/or orbit propagator) would increase the cost, mass, and volume, not being compatible with the 1U CubeSat format.

The analysis focuses on estimating the residual magnetic moment and implementing full magnetic control, with variations on the extended Kalman filter reported in the literature:

1. Nonlinear model for the prediction step, which makes it easier to include arbitrary disturbance models.
2. Estimator integrated with the magnetic feedback, modifying the estimation model transition matrix accordingly, which becomes more relevant for bodies with different principal moments of inertia.
3. Adaptive process covariance matrix, which allows easier filter tuning and faster convergence.

Finally, a specific time varying version of the observability matrix rank condition was verified in order to validate the proposal.

The control law is based on the definition of a partial quaternion associated with the error of a single vector relative to an almost inertial vector reference. This was applied to the sun vector as well as the nadir vector, which gave good enough results by simulations, although the last one is not actually an inertial pointing. In both cases, a high sensitivity to initial conditions was observed on the free rotation about the pointed axis, even without random components on the simulation. This is acceptable from a mission standpoint, as the requirements of these control modes are invariant under these rotations. Future work will consider additional stability analysis to prove that the nadir pointing is asymptotically stable, including the logic to mitigate the lack of information when the horizon is outside the field of view of the sensor.

Author contributions

The authors have contributed equally, read and agreed to the published version of the manuscript.

Use of AI tools declaration

The authors declare they have not used Artificial Intelligence (AI) tools in the creation of this article.

Acknowledgments

This work was supported by the Universidad de Buenos Aires (UBA), Comisión Nacional de Actividades Espaciales (CONAE) and Secretaría de Innovación, Ciencia y Tecnología de Argentina.

Conflict of interest

All authors declare no conflicts of interest in this paper.

References

1. Alarazah HAA, Teofilatto P (2018) Theoretical and Numerical Analysis of the Attitude Control of a 3U CubeSat - Iraqi Satellite (TIGRISAT). *Assoc Arab Univ J Eng Sci* 25: 236–257. https://www.jaaru.org/index.php/auisseng/article/view/207
2. Alvarez D, Aguilar-Nadalini A, Bagur J, et al. (2025) Design and On-Orbit Performance of the Attitude Determination and Passive Control System for the Quetzal-1 CubeSat. *J Small Satell* 12: 1231–1247. Available from: https://jossonline.com.
3. Carletta S, Nascetti A, Gosikere Matadha SS, et al.(2022) Characterization and Testing of the Passive Magnetic Attitude Control System for the 3U AstroBio CubeSat. *Aerospace* 9: 723. https://doi.org/10.3390/aerospace9110723
4. Riano-Rios C, Sun R, Bevilacqua R, et al. (2018) Aerodynamic and gravity gradient based attitude control for CubeSats in the presence of environmental and spacecraft uncertainties. *Acta Astronaut* 180: 439–450. https://doi.org/10.1016/j.actaastro.2020.12.038
5. Sutherland R, Kolmanovsky I, Girard AR (2019) *Attitude Control of a 2U Cubesat by Magnetic and Air Drag Torques*. Ieee T Contr Syst Technol 27: 1047–1059. https://doi.org/10.1109/TCST.2018.2791979
6. Gaude A, Vaios L (2020) Design and Structural Analysis of a Control Moment Gyroscope (CMG) Actuator for CubeSats. *Aerospace* 7: 55. https://doi.org/10.3390/aerospace7050055
7. Grau S, Kapitola S, Weiss S, et al. (2021) Control of an Over-actuated Spacecraft using a Combination of a Fluid Actuator and Reaction Wheels. *Acta Astronautica* 178: 870–880. https://doi.org/10.1016/j.actaastro.2020.10.018
8. Gatsonis N, Lu Y, Blandino J, et al. (2014) Cubesat Design and Attitude Control with Micro Pulsed Plasma Thrusters. *AIAA SPACE 2014 Conference and Exposition*. https://doi.org/10.2514/6.2014-4211
9. Hanisch E, Servidia P (2025) USAT-I Attitude Control System Trade-off Studies, Stability Analysis and oimulations. *Metascience Aerosp* 2: 42–67. https://doi.org/10.3934/mina.2025003
10. Hassan AM, El-Badawy AA (2021) Novel Omnimagnet Actuation Method for a Cubesat Nano-Satellite. *Aerosp Sci Technol* 117: 106913. https://doi.org/10.1016/j.ast.2021.106913
11. Khan SA, Tao Z, Fahad S, et al. (2023) Reliable Attitude Control Integrating Reaction Wheels and Embedded Asymmetric Magnetorquers for Detumbling CubeSats. *Computers & Electrical Engineering.* 74: 5906–5922. https://doi.org/10.1016/j.asr.2024.08.056
12. Lassakeur A, Roubache R, Bekhadda N (2022) A Survey of the Magnetic Dipole Moment Determination Methods Applied on CubeSats and Nanosatellites. *International Astronautical Congress*, Paris, France.
13. Inamori T, Nakasuka S, Sako N (2009) In-orbit Magnetic Disturbance Estimation and Compensation using UKF in Nano-Satellite Mission. *AIAA Guidance, Navigation, and Control Conference*, Chicago, Illinois, US. https://doi.org/10.2514/6.2009-5905
14. Inamori T, Sako N, Nakasuka S (2011) Magnetic Dipole Moment Estimation and Compensation for an Accurate Attitude Control in Nano-satellite Missions. *Acta Astronaut* 68: 2038–2046. https://doi.org/10.1016/j.actaastro.2010.10.022

15. Khalil H (2002) *Nonlinear Systems*, 3rd. edition, Prentice Hall.

16. Lovera M, Astolfi A (2004) Spacecraft Attitude Control using Magnetic Actuators. *Automatica* 40: 1405–1414. https://doi.org/10.1016/j.automatica.2004.02.022

17. Servidia P, Sanchez Peña R (2005) Practical Stabilization in Attitude Thruster Control. *IEEE Transactions on Aerospace and Electronic Systems* 41: 584–598. https://doi.org/10.1109/TAES.2005.1468750

18. ASTAR, (2025) Primeros proyectos institucionales del programa PIT-FIUBA. University of Buenos Aires. Available from: www.fi.uba.ar/noticias/primeros-proyectos-institucionales-del-programa-pit-fiuba.

19. Canepa V, Husain S, Servidia P (2024) Trade-Off Analysis for Attitude Control in Highly Elliptical Orbits. *IEEE ARGENCON 2024*, San Nicolás, Argentina. https://doi.org/10.1109/ARGENCON62399.2024.10735803

20. Ovchinnikov M. Yu., Roldugin D.S., (2019) A Survey on Active Magnetic Attitude Control Algorithms for Small Satellites. *Prog Aerosp Sci* 109: 100546. https://doi.org/10.1016/j.paerosci.2019.05.006

21. Trégouët JF, Arzelier D, Peaucelle D, et al. (2013) Static Input Allocation for Reaction Wheels Desaturation using Magnetorquers, *19th IFAC Symposium on Automatic Control in Aerospace*, IFAC Proceedings Volumes, 46: 559–564, https://doi.org/10.3182/20130902-5-DE-2040.00066

22. Horn RA, Johnson CR (2013) *Matrix Analysis*, Cambridge University Press, 2nd. ed.

23. Della Rossa F, Bergamasco M, Lovera M (2012) Bifurcation analysis of the attitude dynamics for a magnetically controlled spacecraft, *51st IEEE Conference on Decision and Control (CDC)*, 1154–1159. https://doi.org/10.1109/CDC.2012.6426150

24. Ward MJ (2017) *Chapter 3: Basic Floquet Theory*. Available from: www.personal.math.ubc.ca/.

25. Servidia P, Giribet J, España M (2024) Suborbital Ascent Guidance and Control on VEx1B, *IAA Latin American Conference on Small Satellites*, Technology and Applications, Salta, Argentina.

26. Exchange S (2017) Maximum angle between a vector x and its linear transformation Ax. Available from: www.math.stackexchange.com/questions/2266057/maximum-angle-between-a-vector-x-and-its-linear-transformation-a-x.

27. CubeSpace *Horizon Sensor*. Available from: https://www.cubespace.co.za/products/earth-horizon-sensor/.

28. Celani F (2023) Reduced-Attitude Stabilization for Spacecraft Boresight Pointing using Magnetorquers. *Mater Res P* 37: 611–614. https://doi.org/10.21741/9781644902813-133

29. Celani F (2026) Boresight Stabilization of an Earth-Pointing Satellite using Magnetorquers. *Acta Astronaut* 239: 97–112. https://doi.org/10.1016/j.actaastro.2025.11.005

30. Cánepa V, Servidia P, Giribet J (2022) Adaptive Extended Kalman Filter for Integrated Navigation in a Satellite Launch Vehicle, *VI Congreso Bienal de la Sección Argentina del IEEE (ARGENCON)*, San Juan, Argentina. https://doi.org/10.1109/ARGENCON55245.2022.9939949

31. España M, Carrizo J, Giribet J (2019) Sensability and Excitability Metrics Applied to Navigation Systems Assessment. *J Navig* 72: 1481–1495. https://doi.org/10.1017/S0373463319000328

32. Carrara V (2015) An Open Source Satellite Attitude and Orbit Simulator Toolbox for Matlab, *Proceedings of the XVII International Symposium on Dynamic Problems of Mechanics*, Natal, 22–27.
33. Space Academy, Terrestrial atmosphere modelling. Available from: www.spaceacademy.net.au/watch/debris/atmosmod.htm.
34. Vallado DA, McClain WD (2001) *Fundamentals of Astrodynamics and Applications*, 4th. edition, Microcosm Press.
35. Ahmed Khan S, Tao Z, Fahad S, et al. (2024) Reliable attitude control integrating reaction wheels and embedded asymmetricmagnetorquers for detumbling CubeSats. *Adv Space Res* https://doi.org/10.1016/j.asr.2024.08.056.
36. Strogatz S (2015) *Nonlinear Dynamics And Chaos*, CRC Press.

AIMS Press